In: *Proceedings of the SPIE Automatic Object Recognition III Conference*, Orlando, FL, April 1993.

Full polarization two-dimensional Prony modeling with application to radar target identification

Joseph J. Sacchini
Department of Electrical Engineering
Air Force Institute of Technology
WPAFB, OH 45433

William M. Steedly
The Analytic Sciences Corporation
Reston, VA 22090

Randolph L. Moses
Department of Electrical Engineering
The Ohio State University
Columbus, OH 43210

ABSTRACT

A new two-dimensional (2-D) technique is developed to estimate the polarimetric characteristics of scattering centers that exist on radar targets. This technique uses a 2-D damped exponential model to approximate the scattering from radar targets. The validity of this model is investigated relative to the scattering characteristics that exist on the targets of interest. Simulations are shown which validate the technique.

1. INTRODUCTION

A new two-dimensional (2-D) technique is developed to estimate the polarimetric characteristics of scattering centers that exist on radar targets. First, a candidate list of canonical scattering centers is developed. The scattering characteristics of the scattering centers, which consist of the monostatic scattering as a function of frequency, angle, and polarization, are estimated. Next, a new full polarization 2-D parametric model and estimation technique, called the Full Polarization 2-D TLS-Prony Technique, is introduced. This technique is an extension of several already developed.[1,2,3] Damped exponentials are used to model the frequency and angular behavior of the scattering centers. The estimation technique uses a total least squares approach to determine the parameter estimates and a singular value decomposition (SVD) for noise cleaning purposes.[2] From these estimates, the polarimetric characteristics of each individual scattering center are determined using the concept of a Transient Polarization Response (TPR).[4]

Scattering response characteristics of the canonical scattering centers can be generated using techniques such as the Method of Moments and the Geometrical Theory of Diffraction. The candidate list of canonical scattering centers used in this paper is as follows: point scatter, sphere, corner, edge, dihedral, trihedral, right-circular cylinder, and flat plate. Models for each have been developed using the generated scattering responses[5] and are presented here. The frequency and angular behaviors are modeled by damped exponentials. The damped exponential is an accurate model for the frequency behavior of the scattering centers listed while it is not as accurate for the angular behavior, but still accurate enough so that the estimation procedure can obtain good parameter estimates.[5]

The Full Polarization 2-D TLS-Prony Technique models the frequency and angular behavior using a 2-D extension of Prony's Model. The parameters are determined sequentially from the model. First, the scattering center's frequency parameters are estimated, then their angular parameters are estimated, both from the full polarization data. Next, amplitude coefficients are found for each polarization. From these parameters, the polarimetric characteristics are determined. The damped exponential estimates determine the locations of the scattering centers while the amplitude coefficient estimates determine their polarimetric properties. This technique allows a large 2-D full polarization data set to be reduced to a parameter vector consisting of four complex numbers for each scattering center, which in most cases results in a large data reduction. Super-resolution is also achieved using this technique, due to the parametric modeling aspect.

An outline of this paper is as follows. In Section 2 we investigate the electromagnetic behavior of the canonical scattering centers and we develop the scattering center model for a radar target. In Section 3 we describe the Full Polarization 2-D TLS-Prony Technique. Section 4 presents simulations using the technique. Finally, Section 5 concludes the paper.

2. ELECTROMAGNETIC MODELING OF RADAR SCATTERING

2.1 Electromagnetic behavior of canonical scattering centers

Before a target can be broken down into its primary scattering centers, the scattering characteristics of canonical scattering centers must be estimated and modeled. In this paper, the scattering characteristics consist of the monostatic radar return as a function of frequency of illumination, angle of incidence, and transmit and receive polarization for a continuous wave (CW) radar. A great deal of work has been done in the area of plane wave scattering prediction for simple shapes. Exact analytical scattering solutions exist for only a few simple shapes, such as a sphere and an infinite right circular cylinder.

A goal of this work is to develop a list of canonical scattering centers which are commonly found on the radar targets of interest. This list must be based upon knowledge of what basic scattering mechanisms are present on radar targets. Eight canonical scattering centers are presented here. They are the point scatterer, sphere, corner, edge, dihedral, trihedral, right-circular cylinder, and flat plate. This group is not all inclusive for all potential radar targets, but contains scattering centers found on many radar targets. The physical description of the canonical scattering centers are now described. For this work, all of the scatterers are assumed to be perfect conductors. The point scatterer is, by definition, a point. The sphere is a standard spherical shell. The corner, edge, and flat plate are defined in Figure 1(a). The flat plate that the edge and corner lie on is considered infinitesimally thin. A typical dihedral is sketched in Figure 1(b), a typical trihedral in Figure 1(c), and a typical right-circular cylinder in Figure 1(d).

The scattering characteristics of each were analyzed by Sacchini[5] using the available techniques such as the Method of Moments and the Geometrical Theory of Diffraction, and are only summarized here. From this analysis, models were developed to estimate the scattering behavior of each of the canonical scattering centers. These models were determined using two main criteria. First, the models must be simple enough for use in inverse scattering algorithms. Second, they must be as accurate as possible from an electromagnetic standpoint. The model characteristics are listed in Table 1.

Table 1: Approximate Frequency and Angle characteristics of canonical scattering centers.

Scatterer	Frequency Dependence	Angular Dependence
1. Point Scatterer, Sphere	constant	constant
2. Corner, no grazing	ω^{-1}	constant
3. Corner, grazing	ω^{-1}	$\delta_p(\varphi)$
4. Edge, no grazing	constant	constant
5. Edge, grazing	constant	$\delta_p(\varphi)$
6. Dihedral, azimuth scan	ω	$\delta_p(\varphi)$
7. Dihedral, elevation scan	ω	$U(\varphi)$
8. Trihedral	ω	$U(\varphi)$
9. Cylinder, $\theta = 90°$	$\sqrt{\omega}$	$\delta_p(\varphi)$
10. Cylinder, $0° < \theta < 90°$	$\frac{1}{\sqrt{\omega}}$	constant
11. Cylinder, $\theta = 0°$	ω	$\delta_p(\varphi)$
12. Flat Plate (specular)	ω	$\delta_p(\varphi)$

In Table 1, ω is the radian frequency, $U(\varphi)$ is a step function of angle, and $\delta_p(\varphi)$ is an impulse-like function of angle. $U(\varphi)$ is defined as

$$U(\varphi) = \begin{cases} 1, & \varphi \geq 0 \\ 0, & \varphi < 0 \end{cases}, \tag{1}$$

and $\delta_p(\varphi)$ is defined as

$$\delta_p(\varphi) = \begin{cases} 1, & \varphi = 0 \\ 0, & \varphi \neq 0 \end{cases} . \tag{2}$$

Note that φ is an arbitrary angular coordinate which is needed to state the models. For example, from the electromagnetic analysis, it is known that the dihedral in Figure 1(b) has its impulsive type behavior at $\phi = 0°$ and $\theta = 90°$. The variable φ is the angular variable along any angular swath starting at this point, since $\delta_p(\varphi)$ has its impulsive behavior at $\varphi = 0°$.[6] For the canonical scattering centers with impulsive angular behavior, the angle at which the impulsive behavior occurs corresponds to the $\varphi = 0°$ angle. Also, for the canonical scattering centers with a step angular behavior, the angle at which the step behavior occurs corresponds to the $\varphi = 0°$ angle. Of course, for the canonical scattering centers with a constant angular behavior, the origin of the φ coordinate is insignificant. Also note that θ in Table 1 is the θ in the standard spherical coordinate system. and the right circular cylinder's axis is along the z-axis.

For the corner, the angles which are parallel with one of the edges that defines a corner are called the 'grazing' angles. For the edge, the angles which are parallel with or perpendicular to the edge are called the 'grazing' angles.

2.2 Electromagnetically based scattering model for a complicated target

It is assumed that the high frequency scattering from an electrically large complicated target such as an aircraft or a tank can be accurately approximated by a sum of scattering from a finite number of predominant scattering centers.[4,7] The scattering from a complicated target is thus approximated from the following model:

$$\begin{bmatrix} \mathbf{E}_h^s(\omega,\theta,\phi) \\ \mathbf{E}_v^s(\omega,\theta,\phi) \end{bmatrix} = \sum_{\gamma=1}^{\Gamma} \mathbf{S}_\gamma(\omega,\theta,\phi) \begin{bmatrix} \mathbf{E}_h^i(\omega,\theta,\phi) \\ \mathbf{E}_v^i(\omega,\theta,\phi) \end{bmatrix} \left(\frac{e^{-jk_o r}}{r}\right), \tag{3}$$

where

$$\mathbf{S}_\gamma(\omega,\theta,\phi) = \begin{bmatrix} \mathrm{s}_{hh}^\gamma(\omega,\theta,\phi) & \mathrm{s}_{hv}^\gamma(\omega,\theta,\phi) \\ \mathrm{s}_{vh}^\gamma(\omega,\theta,\phi) & \mathrm{s}_{vv}^\gamma(\omega,\theta,\phi) \end{bmatrix} \tag{4}$$

is the scattering matrix for the γ-th scattering center on the target, and where $\mathbf{E}_h^i(\omega,\theta,\phi)$, $\mathbf{E}_v^i(\omega,\theta,\phi)$, $\mathbf{E}_h^s(\omega,\theta,\phi)$, and $\mathbf{E}_v^s(\omega,\theta,\phi)$ are the incident and scattered horizontally and vertically polarized electric fields, respectively. Also, θ and ϕ are the standard spherical coordinates in a target fixed coordinate system (the target is located at the origin of the coordinate system). $\mathbf{S}_\gamma$ can be further decomposed as

$$\mathbf{S}_\gamma(\omega,\theta,\phi) = \begin{bmatrix} \mathbf{p}_{hh}^\gamma(\theta,\phi) & \mathbf{p}_{hv}^\gamma(\theta,\phi) \\ \mathbf{p}_{vh}^\gamma(\theta,\phi) & \mathbf{p}_{vv}^\gamma(\theta,\phi) \end{bmatrix} F_\gamma(\omega)\, e^{-jk_o r_\gamma} \tag{5}$$

or

$$\mathbf{S}_\gamma(\omega,\theta,\phi) = \mathbf{P}_\gamma(\theta,\phi)\, F_\gamma(\omega)\, e^{-jk_o r_\gamma}. \tag{6}$$

$\mathbf{P}_\gamma$ will be called the polarization matrix and is not a function of frequency. All of the terms in Equation (6), namely, $\mathbf{S}_\gamma$, $\mathbf{P}_\gamma$ and $F_\gamma(\omega)$, are, in general, complex. The distance between the phase center of the target and the arbitrarily designated phase center of the γ-th scattering center, projected along the radar's line of sight, is given by r_γ. Note that r_γ is an implicit function of θ and ϕ. It is assumed that there are Γ scattering centers on the target. It is also worth noting that this is a full polarization scattering model.

The electromagnetic analysis has demonstrated that for the canonical scattering centers analyzed here, factoring out the frequency dependence as a scalar from the remainder of the scattering matrix is reasonable.[5] However, factoring out the angular dependencies as scalar functions turns out to be a poor assumption for canonical scattering centers such as the corner and the edge.[5] Of course, for physically symmetric scattering centers such as a sphere, the angular dependence could be separated from the rest of the scattering matrix. Most radar targets of interest contain many corners and edges, and thus a model that factors out the angular dependence from the rest of the scattering

matrix would not exactly model the phenomena which is occurring. The damped exponential model we introduce in the next does factor out the angular dependence, but this drawback is not significant enough to preclude the use of this model, as is demonstrated in the simulations in Section 4.

2.3 Damped exponential modeling of canonical scattering centers

Another model which can be used to approximate the scattering from a radar target is the damped exponential model given by

$$d(m,n) = \sum_{\gamma=1}^{\Gamma} \alpha_\gamma \rho_{x_\gamma}^m \rho_{y_\gamma}^n \tag{7}$$

where

$$\begin{aligned} \rho_{x_\gamma} &= \gamma\text{th } x\text{-pole, } x\text{-component of 2-D exponential (complex number)} \\ \rho_{y_\gamma} &= \gamma\text{th } y\text{-pole, } y\text{-component of 2-D exponential (complex number)} \\ \alpha_\gamma &= \gamma\text{th amplitude coefficient (complex number)} \\ \Gamma &= \text{number of scattering centers (integer)} \end{aligned}$$

and where $m = 0, 1, \ldots M-1$ and $n = 0, 1, \ldots N-1$. This is a 2-D extension of Prony's Model. This model assumes the radar target is comprised of Γ scattering centers. The γ-th scattering center's scattering behavior, for a single transmit and receive polarization, is modeled by the x-pole, y-pole, and amplitude coefficient triple, $\{\rho_{x_\gamma}, \rho_{y_\gamma}, \alpha_\gamma\}$. The magnitude of the x-component damped exponential, $|\rho_{x_\gamma}|$, determines the dispersion of the γ-th scattering center in the x-coordinate of the transform domain (time or range domain in this case) while the angle of the x-component damped exponential, $\angle\rho_{x_\gamma}$, determines the location of the γ-th scattering center in the x-coordinate of the transform domain. Similarly, the magnitude of the y-component damped exponential, $|\rho_{y_\gamma}|$, determines the dispersion of the γ-th scattering center in the y-coordinate of the transform domain while the angle of the y-component damped exponential, $\angle\rho_{y_\gamma}$, determines the location of the γ-th scattering center in the y-coordinate of the transform domain.

From Equations (3) and (6), we see that a single polarization version for the scattering from a complicated target is given by

$$\mathbf{E}_x^s(\omega,\theta,\phi) = \sum_{\gamma=1}^{\Gamma} \mathbf{p}_{xy}^\gamma(\theta,\phi) F_\gamma(\omega) \mathbf{E}_y^i(\omega,\theta,\phi) \left(\frac{e^{-jk_o r}}{r}\right) \tag{8}$$

where $x \in \{h,v\}$, $y \in \{h,v\}$ and $xy \in \{hh, hv, vv\}$. Comparing Equations (7) and (8), we see that the γ-th individual scattering center's frequency and angular dependencies are modeled by two damped exponentials, ρ_{x_γ} for the frequency dependence, and ρ_{y_γ} for the angular dependence. Note that there are two angular dependencies in Equation (8), θ and ϕ. When data is taken by a radar, it is taken over a specific angular swath, and this angular swath is a function of both θ and ϕ, but it can be parameterized by the singular angular variable ψ. Thus, there is really only one angular variable over which a 2-D radar data set is taken. There is also an amplitude coefficient associated with the γ-th scattering center in Equation (7), α_γ, which accounts for the remaining terms in Equation (8) (namely, the incident field value, $\mathbf{E}_y^i(\omega,\theta,\phi)$, which is usually constant and equal to 1, the $\frac{e^{-jk_o r}}{r}$ term, the amplitude differences between the angular variable $\mathbf{p}^\gamma(\theta,\phi)$ and ρ_{y_γ}, and the amplitude differences between the frequency variable $F(\omega)$ and ρ_{x_γ}). These relationships are summarized in Table 2. Recall that the terms $F_\gamma(\omega)$ and $\mathbf{p}_{xy}^\gamma(\theta,\phi)$ are, in general, complex.

The frequency dependencies of canonical scattering centers are well modeled using the damped exponentials.[5] However, only one of the angular dependencies, that of constant, is well modeled. The other two, that of $U(\varphi)$ and $\delta_p(\varphi)$, are not well modeled by damped exponentials.[5] Even though the damped exponential does not model all of the scattering centers well, it is still an improvement in the modeling of radar scattering. Much of the previous work in RTI assumed a point scatterer model for the scattering from all types of canonical scattering centers. The extension to a 2-D damped exponential model is an improvement over the point scatterer model.

Table 2: Correspondence between terms in damped exponential scattering model and electromagnetically based scattering model. Note that $xy \in \{hh, hv, vv\}$ and $y \in \{h, v\}$.

Term	Electromagnetic Model	Damped Exp. Model
Frequency	$F_\gamma(\omega)$	ρ_{x_γ}
Angle	$\mathbf{p}_{xy}^{\gamma}(\theta, \phi)$	ρ_{y_γ}
Amplitude	$\frac{e^{-jk_o r}}{r}$, $\mathbf{E}_y^i(\omega, \theta, \phi)$, and amp. diffs.	α_γ

3. THE FULL POLARIZATION TWO-DIMENSIONAL TLS-PRONY TECHNIQUE

The Full Polarization 2-D TLS-Prony Technique is a parametric technique for the estimation of 2-D exponentials and their associated amplitude coefficients. The model used for the data is a 2-D extension of the 1-D Full Polarization Prony model introduced by Steedly.[8] This model is also given in Equation (7). The estimation procedure is an extension of the estimation procedure developed by Steedly.[1] Prony's method coupled with a total least squares (TLS) technique in 1-D has been successfully used to estimate frequencies in the presence of noise.[2] With the Full Polarization 2-D TLS-Prony Technique, 2-D exponentials and amplitude coefficients are estimated by a two-step method using a 1-D TLS-based Prony model and estimation technique in each step.

A method to examine full polarization data is presented here which is based on the concept of a Transient Polarization Response (TPR).[4] According to the TPR concept, the target is illuminated with an impulsive circularly polarized electromagnetic wave, and as the wave interacts with each scattering center on the target, each scattering center will reflect back a wave with a polarization which is determined by the polarimetric characteristics of that scattering center. This concept has been investigated in 1-D for both nonparametric[4] and parametric[8] techniques. The nonparametric techniques use the IFFT of the full polarization stepped frequency data to form the TPR of a target. The peaks in the TPR profile give the scattering center locations. Polarization ellipses are then given by the polarization properties of the TPR at the scattering center locations. Thus, the amplitude and orientation of each ellipse characterize the polarimetric properties of each scattering center. Parametric techniques employing the 1-D TLS-Prony technique have been developed for the TPR.[8] This technique has the advantage of higher resolution than the IFFT method and of direct estimation of the scattering center locations.

The technique presented here is a 2-D extension of the 1-D TLS-Prony based parametric TPR technique developed by Steedly.[8] The 2-D TLS-Prony Technique algorithms presented by Sacchini, *et. al.*,[1] with some modifications, are used to determine the scattering center locations and amplitude coefficients. The ellipse parameters are then calculated from the amplitude coefficients.

3.1 Data model

Assume that we are given full polarization, 2-D scattering coefficient data. These coefficients are denoted $\mathbf{s}_{hh}(f, \psi)$, $\mathbf{s}_{hv}(f, \psi) = \mathbf{s}_{vh}(f, \psi)$, and $\mathbf{s}_{vv}(f, \psi)$, where ψ is the angular variable along the angular path on which the data was taken. Depending upon the locations of the samples in the 2-D frequency plane, the scattering coefficients can serve as the input data to the 2-D TLS-Prony algorithm. However, the algorithm requires data which lies on a rectangular or square grid in the 2-D frequency plane. It may be desirable to interpolate the data which lies on the polar grid onto a square or rectangular grid. In either case, the data which is input to this algorithm is denoted as $d'_{hh}(m, n)$, $d'_{hv}(m, n) = d'_{vh}(m, n)$, and $d'_{vv}(m, n)$ where $m = 0, 1, \ldots M-1$ and $n = 0, 1, \ldots N-1$ and the $'$ denotes that the data has been noise corrupted. The first index, m, is referred to as the x-component, and the second index, n, as the y-component. The x-component is analogous to the frequency component and the y-component is analogous to the angular component in the 2-D frequency plane.

The 2-D TPR can be modeled in the 2-D frequency domain as

$$\begin{bmatrix} d_{hh}(m,n) & d_{hv}(m,n) \\ d_{vh}(m,n) & d_{vv}(m,n) \end{bmatrix} = \sum_{k=1}^{K} \sum_{l=1}^{L_k} \begin{bmatrix} a_{hh_{k,l}} & a_{hv_{k,l}} \\ a_{vh_{k,l}} & a_{vv_{k,l}} \end{bmatrix} p_{x_k}^m p_{y_{k,l}}^n \tag{9}$$

where

$$\begin{aligned}
p_{x_k} &= k\text{th } x\text{-pole, } x\text{-component of the 2-D exponential} \\
p_{y_{k,l}} &= k,l\text{th } y\text{-pole, } y\text{-component of the 2-D exponential} \\
a_{hh_{k,l}} &= k,l\text{th linear basis amplitude coefficient for } hh\text{-polarization} \\
a_{vh_{k,l}} &= k,l\text{th linear basis amplitude coefficient for } vh\text{-polarization} \\
a_{hv_{k,l}} &= k,l\text{th linear basis amplitude coefficient for } hv\text{-polarization} \\
a_{vv_{k,l}} &= k,l\text{th linear basis amplitude coefficient for } vv\text{-polarization} \\
K &= \text{number of } x\text{-poles} \\
L_k &= \text{number of } y\text{-poles corresponding to the } k\text{th } x\text{-pole.}
\end{aligned}$$

This is designated the linear-basis model. Note that due to reciprocity, $a_{hv_{k,l}}$=$a_{vh_{k,l}}$. Also note that this is the same model as the one given in Equation (7), with the summation just written in a different form in order to more easily explain the estimation algorithm.

The polarization properties of each scattering center are more clearly seen by considering the horizontal and vertical responses to a circularly polarized incident wave. Left circular is arbitrarily chosen. It is assumed that there are no helical type scattering centers on the target which would cause the left and right circular responses to be different. Thus, the data is reduced from four sets to two by the transformation[4]

$$\begin{bmatrix} d_{hl}(m,n) \\ d_{vl}(m,n) \end{bmatrix} = \begin{bmatrix} d_{hh}(m,n) & d_{hv}(m,n) \\ d_{vh}(m,n) & d_{vv}(m,n) \end{bmatrix} \begin{bmatrix} 1 \\ j \end{bmatrix} \frac{1}{\sqrt{2}}. \tag{10}$$

The 2-D full polarization model can also be written in terms of the hl and vl-polarization based data as

$$\begin{bmatrix} d_{hl}(m,n) \\ d_{vl}(m,n) \end{bmatrix} = \sum_{k=1}^{K} \sum_{l=1}^{L_k} \begin{bmatrix} a_{h_{k,l}} \\ a_{v_{k,l}} \end{bmatrix} p_{x_k}^m p_{y_{k,l}}^n \tag{11}$$

where

$$\begin{aligned}
a_{h_{k,l}} &= k,l\text{th horizontal amplitude coefficient for } hl\text{-polarization} \\
a_{v_{k,l}} &= k,l\text{th vertical amplitude coefficient for } vl\text{-polarization.}
\end{aligned}$$

This is designated the linear-circular basis model. Note that p_{x_k} and $p_{y_{k,l}}$ are identical to the poles for the linear-basis model.

The problem now becomes one of parameter estimation, where the parameters in Equation (11), namely p_{x_k}, $p_{y_{k,l}}$, $a_{h_{k,l}}$ and $a_{v_{k,l}}$ for $k = 1, 2, \ldots, K$ and $l = 1, 2, \ldots, L_k$ must be estimated from the data. The model orders, K and L_k also need to be chosen.

The horizontal and vertical amplitude coefficients associated with each pole contain the information which yields the polarimetric characteristics of each scattering center. These polarimetric characteristics are in the form of an ellipse. This ellipse, corresponding to a given scattering center, is characteristic of the polarization of the electric field scattered from that scattering center. For each scattering center, the tilt, $\tau_{k,l}$, and ellipticity, $\epsilon_{k,l}$, of this ellipse can be found, using the amplitude coefficients, from the following equations:[4]

$$\tau_{k,l} = \frac{1}{2} \tan^{-1} \left[\tan(2\gamma_{k,l}) \cos(\delta_{k,l}) \right] \tag{12}$$

$$\epsilon_{k,l} = \frac{1}{2}\sin^{-1}\left(\sin(2\gamma_{k,l})\sin(\delta_{k,l})\right), \tag{13}$$

where

$$\gamma_{k,l} = \tan^{-1}\left(\frac{|a_{v_{k,l}}|}{|a_{h_{k,l}}|}\right) \tag{14}$$

$$\delta_{k,l} = \angle a_{v_{k,l}} - \angle a_{h_{k,l}}. \tag{15}$$

The above calculations lead to use of only one quarter of the Poincaré polarization sphere. To avoid this ambiguity, the following alterations to the tilt need to be made:[4]

$$\tau_{k,l} = \begin{cases} \tau_{k,l} + \frac{\pi}{2} & \text{if } \gamma_{k,l} > \frac{\pi}{4} \\ \tau_{k,l} + \pi & \text{if } \gamma_{k,l} \leq \frac{\pi}{4} \text{ and } \tau_{k,l} < 0 \end{cases} \tag{16}$$

The major axis $A_{k,l}$ of each ellipse can be determined as[4]

$$A_{k,l} = \left||a_{h_{k,l}}|\cos(\tau_k) + |a_{v_{k,l}}|e^{j\,\delta_{k,l}}\sin(\tau_{k,l})\right|. \tag{17}$$

This set of parameters, $\{A_{k,l}, \epsilon_{k,l}, \tau_{k,l}\}$, along with the locations of the scattering centers, provides a concise description of a target. This parameter set characterizes a target as a set of Γ scattering centers, each described by location, amplitude, ellipticity and tilt of a scattering polarization ellipse. The location of the scattering center determines where on the image the ellipse is placed. The origin of the ellipse is considered the location of the scattering center.

The definitions of the ellipse parameters given above are consistent with the IEEE standard for the polarization of an electromagnetic wave which is viewing the tip of the electric field vector as the electric field propagates away from the viewer. However, in the simulations which are shown, it is desired to view the scattered field as it propagates toward the viewer, which corresponds to how the radar would view the scattered field. All of the ellipses plotted in this paper follow the convention of assuming that the viewer is at the radar and the scattered field is propagating toward the radar.

3.2 Estimation algorithms

This section describes two algorithms for estimation of the x and y-poles along with both sets of amplitude coefficients. The two full polarization algorithms are called Full Polarization Algorithm One (FPA1) and Full Polarization Algorithm Two (FPA2). As you will see, FPA2 is more accurate, yet more computationally burdensome, than FPA1. We assume that we are given horizontal (hl-polarized data) and vertical (vl-polarized data) data matrices defined as follows

$$D'_h = \begin{bmatrix} d'_{hl}(0,0) & d'_{hl}(1,0) & \cdots & d'_{hl}(M-1,0) \\ d'_{hl}(0,1) & d'_{hl}(1,1) & \cdots & d'_{hl}(M-1,1) \\ \vdots & \vdots & & \vdots \\ d'_{hl}(0,N-1) & d'_{hl}(1,N-1) & \cdots & d'_{hl}(M-1,N-1) \end{bmatrix} \tag{18}$$

and

$$D'_v = \begin{bmatrix} d'_{vl}(0,0) & d'_{vl}(1,0) & \cdots & d'_{vl}(M-1,0) \\ d'_{vl}(0,1) & d'_{vl}(1,1) & \cdots & d'_{vl}(M-1,1) \\ \vdots & \vdots & & \vdots \\ d'_{vl}(0,N-1) & d'_{vl}(1,N-1) & \cdots & d'_{vl}(M-1,N-1) \end{bmatrix}. \tag{19}$$

Moving across a row in D'_h or D'_v is considered moving in frequency while moving down a column of either matrix is considered moving in angle in the 2-D frequency plane.

3.2.1 Full Polarization Algorithm One (FPA1)

The five steps of FPA1 are described below. The x-poles, $\{p_{x_k}\}_{k=1}^{K}$, are first estimated using a TLS-Prony algorithm. Second, a set of amplitude coefficients corresponding to these x-pole estimates are computed. The amplitude coefficients are themselves used in a set of second TLS-Prony estimates to obtain the y-pole estimates, $\{p_{y_{k,l}}\}_{k,l=1}^{K,L_k}$, which is the third step. Finally, a least squares technique is used to estimate the amplitude coefficients $\{a_{k,l}\}_{k,l=1}^{K,L_k}$.

FPA1 Step 1, estimation of the x-poles, p_{x_k}: All of the rows of D'_h and D'_h are used simultaneously in the estimation of the x-poles. The backward linear prediction equations are given by

$$\left[\begin{array}{ccccc}
d'_{hl}(0,0) & d'_{hl}(1,0) & d'_{hl}(2,0) & \cdots & d'_{hl}(Q,0) \\
d'_{hl}(1,0) & d'_{hl}(2,0) & d'_{hl}(3,0) & \cdots & d'_{hl}(Q+1,0) \\
\vdots & \vdots & \vdots & & \vdots \\
d'_{hl}(M-Q-1,0) & d'_{hl}(M-Q,0) & d'_{hl}(M-Q+1,0) & \cdots & d'_{hl}(M-1,0) \\
\hline
d'_{hl}(0,1) & d'_{hl}(1,1) & d'_{hl}(2,1) & \cdots & d'_{hl}(Q,1) \\
d'_{hl}(1,1) & d'_{hl}(2,1) & d'_{hl}(3,1) & \cdots & d'_{hl}(Q+1,1) \\
\vdots & \vdots & \vdots & & \vdots \\
d'_{hl}(M-Q-1,1) & d'_{hl}(M-Q,1) & d'_{hl}(M-Q+1,1) & \cdots & d'_{hl}(M-1,1) \\
\hline
 & & \vdots & & \\
\hline
d'_{hl}(0,N-1) & d'_{hl}(1,N-1) & d'_{hl}(2,N-1) & \cdots & d'_{hl}(Q,N-1) \\
d'_{hl}(1,N-1) & d'_{hl}(2,N-1) & d'_{hl}(3,N-1) & \cdots & d'_{hl}(Q+1,N-1) \\
\vdots & \vdots & \vdots & & \vdots \\
d'_{hl}(M-Q-1,N-1) & d'_{hl}(M-Q,N-1) & d'_{hl}(M-Q+1,N-1) & \cdots & d'_{hl}(M-1,N-1) \\
\hline\hline
d'_{yl}(0,0) & d'_{yl}(1,0) & d'_{yl}(2,0) & \cdots & d'_{vl}(Q,0) \\
d'_{vl}(1,0) & d'_{vl}(2,0) & d'_{vl}(3,0) & \cdots & d'_{vl}(Q+1,0) \\
\vdots & \vdots & \vdots & & \vdots \\
d'_{vl}(M-Q-1,0) & d'_{vl}(M-Q,0) & d'_{vl}(M-Q+1,0) & \cdots & d'_{vl}(M-1,0) \\
\hline
d'_{yl}(0,1) & d'_{yl}(1,1) & d'_{yl}(2,1) & \cdots & d'_{vl}(Q,1) \\
d'_{vl}(1,1) & d'_{vl}(2,1) & d'_{vl}(3,1) & \cdots & d'_{vl}(Q+1,1) \\
\vdots & \vdots & \vdots & & \vdots \\
d'_{vl}(M-Q-1,1) & d'_{vl}(M-Q,1) & d'_{vl}(M-Q+1,1) & \cdots & d'_{vl}(M-1,1) \\
\hline
 & & \vdots & & \\
\hline
d'_{yl}(0,N-1) & d'_{yl}(1,N-1) & d'_{yl}(2,N-1) & \cdots & d'_{vl}(Q,N-1) \\
d'_{vl}(1,N-1) & d'_{vl}(2,N-1) & d'_{vl}(3,N-1) & \cdots & d'_{vl}(Q+1,N-1) \\
\vdots & \vdots & \vdots & & \vdots \\
d'_{vl}(M-Q-1,N-1) & d'_{vl}(M-Q,N-1) & d'_{vl}(M-Q+1,N-1) & \cdots & d'_{vl}(M-1,N-1)
\end{array}\right]
\left[\begin{array}{c} 1 \\ b_1 \\ b_2 \\ \vdots \\ b_Q \end{array}\right] \approx 0. \tag{20}$$

or

$$S \left[\begin{array}{c} 1 \\ b \end{array}\right] \approx 0, \tag{21}$$

where Q is the order of prediction for the x-poles, and b is the coefficient vector of the polynomial $B(z)$ given by

$$B(z) = 1 + b_1 z + b_2 z^2 + \cdots + b_Q z^Q. \tag{22}$$

Q can be any integer greater than or equal to K, while in practice choosing $Q > K$ results in more accurate parameter estimates.[9] Note that all of the rows of D'_h and D'_v are used simultaneously to estimate a single set of prediction coefficients (and therefore, a single set of x-poles).

The TLS-Prony method considers the effect of noise perturbation of all of the S matrix, and the TLS solution attempts to minimize the effect of these perturbations on the prediction coefficient vector b.[2,10] This is accomplished by taking an SVD of the matrix S and truncating all but the first K singular values to arrive at an estimate $\widehat{S}$.[2,10]

Inserting $\widehat{S}$ in Equation (21) gives the modifies linear predication equation

$$\widehat{S}\begin{bmatrix} 1 \\ b \end{bmatrix} = 0, \tag{23}$$

from which the linear prediction coefficient vector estimate $\widehat{b}$ is found as

$$\widehat{b} = -\widehat{S_2}^{+}\widehat{s_1}, \tag{24}$$

where s_1 is the first column of S and S_2 are the remaining columns and $^+$ denotes the Moore-Penrose pseudo-inverse. A numerically robust solution for $\widehat{b}$ can be found directly from the SVD of S.[2] Finally, the estimates for the x-poles are found by

$$\widehat{p}_{x_q} = \text{zero}_q\left(\widehat{B}(z)\right), \qquad q = 1, 2, \ldots, Q. \tag{25}$$

Because only K singular values of $\widehat{S}$ are nonzero, there are at most K x-pole estimates which can correspond to data modes. Therefore, only the K x-poles which have the largest energy will be retained (as discussed in Step 2 below).

FPA1 Step 2, estimation of the x-amplitude coefficients: Before the y-poles are estimated, the x-amplitude coefficients must first be estimated. For the full polarization case, the x-amplitude coefficients are defined as

$$\begin{bmatrix} c_{h_{q,n}} \\ c_{v_{q,n}} \end{bmatrix} = \sum_{l=1}^{L_k} \begin{bmatrix} a_{h_{k,l}}(m,n) \\ a_{v_{k,l}}(m,n) \end{bmatrix} p_{y_{q,l}}^n, \qquad q = 1, 2, \ldots, Q. \tag{26}$$

With this definition, the model associated with Equation (11) using the estimated x-poles is written as

$$\begin{bmatrix} d'_{hl}(m,n) \\ d'_{vl}(m,n) \end{bmatrix} = \sum_{q=1}^{Q} \begin{bmatrix} c_{h_{q,n}} \\ c_{v_{q,n}} \end{bmatrix} p_{x_q}^m \tag{27}$$

where $c_{h_{q,n}}$ is the qth x-amplitude coefficient associated with the nth row of D_h and where $c_{v_{q,n}}$ is the qth x-amplitude coefficient associated with the nth row of D_v.

Note that the equations in (27) are uncoupled for different values of n. Thus, each row of D'_h and each row of D'_v will give an x-amplitude coefficient estimate for each x-pole. The x-amplitude coefficients are an intermediate step in the estimation procedure and are completely defined in Equation (27). Also note that the y-pole model orders, $\{L_k\}_{k=1}^K$, may be different for each of the K x-poles. Equation (27) is used to solve for the $c_{h_{q,n}}$s and $c_{v_{q,n}}$s using

$$\begin{bmatrix} 1 & 1 & \cdots & 1 \\ p_{x_1} & p_{x_2} & \cdots & p_{x_Q} \\ p_{x_1}^2 & p_{x_2}^2 & \cdots & p_{x_Q}^2 \\ \vdots & \vdots & & \vdots \\ p_{x_1}^{M-1} & p_{x_2}^{M-1} & \cdots & p_{x_Q}^{M-1} \end{bmatrix} \begin{bmatrix} c_{\eta_{1,0}} & c_{\eta_{1,1}} & \cdots & c_{\eta_{1,N-1}} \\ c_{\eta_{2,0}} & c_{\eta_{2,1}} & \cdots & c_{\eta_{2,N-1}} \\ \vdots & \vdots & & \vdots \\ c_{\eta_{Q,0}} & c_{\eta_{Q,1}} & \cdots & c_{\eta_{Q,N-1}} \end{bmatrix} = {D'_\eta}^T, \tag{28}$$

or

$$P_x C_\eta = {D'_\eta}^T. \tag{29}$$

where

$$\eta \in \{h, v\}. \tag{30}$$

Both initial sets of x-amplitude coefficients are found from least squares solutions to Equation (29) using the x-pole estimates; this can be written as

$$\widehat{C}_\eta = \left(\widehat{P}_x^H \widehat{P}_x\right)^{-1} \widehat{P}_x^H {D'_\eta}^T, \tag{31}$$

although numerically more robust solutions (using, *e.g.*, the QR decomposition) are preferred to direct computation of Equation (31).

We retain only the K x-pole estimates with the highest energy, where the energy is defined as

$$E_q = \sum_{n=0}^{N-1} \left(\left| \widehat{c}_{h_{q,n}} \right|^2 + \left| \widehat{c}_{v_{q,n}} \right|^2 \right) \sum_{m=0}^{M-1} \left| \widehat{p}_{x_q} \right|^{2m} \qquad q = 1, 2, \ldots, Q. \tag{32}$$

The final x-amplitude coefficient estimates are found using a procedure identical to the one used to determine the initial of x-amplitude coefficient estimates outlined above. The only difference is that there are only K x-poles which are used in Equation (28). Also, there are only L_k x-amplitude coefficients (per polarization) to be estimated for each of the K x-poles.

Note that the final set of x-amplitude coefficients are estimated from the K true x-pole estimates, as opposed to simply taking the initial set of x-amplitude coefficients which correspond to the K highest energy modes. This re-estimation of x-amplitude coefficients should allow the parameter estimates (when used in the model in Equation (7)) to better model the original data.

The x-amplitude coefficients serve as the input data to the second Prony model which determines the y-pole locations and ultimately the amplitude coefficients. For each x-pole, there are two sets of N x-amplitude coefficients, each corresponding to a different y-direction data set (a different column of D'_h or D'_v) and a different polarization. The x-amplitude coefficients hold the information which yields the y-pole's locations in the transform domain.

FPA1 Step 3, estimation of the y-poles: The x-amplitude coefficient estimates are now used to solve for the y-pole estimates. For each of the K high energy x-poles, the backward linear prediction equations for the model given by Equation (26) become

$$\begin{bmatrix} c_{h_{k,0}} & c_{h_{k,1}} & \cdots & c_{h_{k,R_k}} \\ c_{h_{k,1}} & c_{h_{k,2}} & \cdots & c_{h_{k,R_k+1}} \\ \vdots & \vdots & & \vdots \\ c_{h_{k,N-R_k-1}} & c_{h_{k,N-R_k}} & \cdots & c_{h_{k,N-1}} \\ \hline c_{v_{k,0}} & c_{v_{k,1}} & \cdots & c_{v_{k,R_k}} \\ c_{v_{k,1}} & c_{v_{k,2}} & \cdots & c_{v_{k,R_k+1}} \\ \vdots & \vdots & & \vdots \\ c_{v_{k,N-R_k-1}} & c_{v_{k,N-R_k}} & \cdots & c_{v_{k,N-1}} \end{bmatrix} \begin{bmatrix} 1 \\ b_1^k \\ b_2^k \\ \vdots \\ b_{R_k}^k \end{bmatrix} \approx 0 \qquad k = 1, 2, \ldots, K \tag{33}$$

or

$$F^{R_k} \begin{bmatrix} 1 \\ b^k \end{bmatrix} \approx 0 \tag{34}$$

where R_k is the order of prediction for the y-poles, and b^k is the coefficient vector of the polynomial $B^k(z)$ given by

$$B^k(z) = 1 + b_1^k z + b_2^k z^2 + \cdots + b_{R_k}^k z^{R_k}. \tag{35}$$

R_k can be any integer greater than or equal to L_k, while in practice choosing $R_k > L_k$ results in more accurate parameter estimates.[9]

Equation (34) is used to solve for the estimate of b^k, $\widehat{b}^k$, in a total least squares sense, analogous to the manner described in FPA1 Step 1, to arrive at a minimum norm (TLS) estimate, where the $R_k + 1 - L_k$ singular values of F^k are truncated to arrive at a noise cleaned estimate $\widehat{F}^k$ (see FPA1 Step 1 for details).

Using this definition, the model in Equation (11) can be expressed as

$$\begin{bmatrix} d_{hl}(m,n) \\ d_{vl}(m,n) \end{bmatrix} = \sum_{\gamma=1}^{\Gamma} \begin{bmatrix} \alpha_{h_\gamma} \\ \alpha_{v_\gamma} \end{bmatrix} \rho_{x_\gamma}^m \rho_{y_\gamma}^n \tag{38}$$

The two sets of amplitude coefficients, one corresponding to each polarization, are found from a least squares solution using Equation (38). Finally, the ellipse parameters are calculated from the pole and amplitude coefficient estimates using Equations (12) to (17).

4. SIMULATIONS

In order to demonstrate the utility and the limitations of the Full Polarization 2-D TLS-Prony Technique, full polarization radar scattering data is analyzed here. The structure analyzed is a thin metal perfectly conducting square plate 0.5 meters long on a side. For the plate, multiple frequency, multiple angle, full polarization data is utilized. For a specific polarization, aspect angle, and frequency, a data point is the complex number corresponding to the magnitude and phase difference between the electromagnetic wave incident on the target radiated by the continuous-wave (CW) radar and the electromagnetic wave received back at the radar. This is consistent with the definition of the scattering matrix in Equations (3) and (4). Thus, we are using samples of the scattering matrix for equally spaced discrete frequencies and discrete angles. This is exactly the data that could be collected by a coherent, focused, spotlight mode Synthetic Aperture Radar (SAR).

The plate is oriented as shown in Figure 2, with the radar located in the xy-plane. The scattering data was simulated using the GTD-based code described by Marhefka.[6] All of the scattering mechanisms which are modeled by the GTD code were used to generate the data. For example, the corner scattering coefficients, the edge scattering coefficients and the double-bounce coefficients are included in the data set. However, the corner scattering coefficients are the dominant terms in the data.

The locations, damping factors, and polarimetric properties of the scattering centers which exist on the plate are estimated using the Full Polarization TLS-Prony Technique. This structure contains corners and edges at both grazing and non-grazing angles. Thus, the ability of the 2-D TLS-Prony Technique to estimate non-point scatterer type scattering centers is demonstrated.

The data sets analyzed consist of the full polarization monostatic scattering matrix from the plate for incidence angles of $-7.5° < \phi < 97.5°$ with θ fixed at 90°, where θ and ϕ are the standard spherical coordinate angles.[5] The frequency range is from 9 GHz to 9.48 GHZ in 16 MHz steps. The angular step size is 0.1°. Each data set is thus 31×31 (number of frequencies × number of angles). This corresponds to a 3° polar swath of data. The unambiguous range for this data set is 9.3684 meters in each direction. Note that this data, which lies on the polar grid, is used directly by the 2-D TLS-Prony Technique, without being interpolated onto a square grid. It is assumed that since these polar data sets are over a relatively small angular swath (3°) and small bandwidth (5%), it is a reasonable approximation to assume that the polar grid is close enough to a square grid to treat the data as if it lies on a square grid. The results are shown in Figure 3.

The polarimetric characteristics of the scattering centers are represented by polarization ellipses calculated from the pole and amplitude coefficient estimates as discussed in Section 3. The plotting of the ellipses on the image plane requires a quantity called the ellipse factor. The units of the amplitude coefficients (which are the same as the scattering coefficients) are in meters. Due to the small magnitude of the scattering coefficients (nominally around 10^{-3} meters), the size of the ellipses must be scaled up in order to view them on the plots. Thus, the ellipse factor is the dimensionless ratio of the size of the ellipses as viewed on the plots which follow to the actual size of the ellipses.

Examining all of the plots involving the plate, it can be seen that the ellipses yield some physical information concerning the scattering centers. For the $\phi = 0°$ case, the ellipses on the leading edge of the plate are oriented parallel to the edge, as is expected from electromagnetic theory.[6] Also, for the $\phi = 90°$ case, the ellipses on the leading

edge are lines oriented in the same direction as the edge. This is also as expected from electromagnetic theory.[6] The intent of this analysis is to provide physical characteristics associated with scattering centers on a radar target. The polarization ellipses accomplish this by displaying the polarimetric characteristics of each scattering center.

5. CONCLUSIONS

This paper developed a new 2-D technique to estimate the polarimetric characteristics of scattering centers that exist on radar targets. First, a candidate list of canonical scattering centers was developed and the scattering characteristics of the scattering centers were estimated. Next, a new full polarization 2-D parametric model and estimation technique, called the Full Polarization 2-D TLS-Prony Technique, was introduced. This technique is an extension of several already developed. Damped exponentials were used to model the frequency and angular behavior of the scattering centers. The estimation technique used a total least squares approach to determine the parameter estimates. From these estimates, the polarimetric characteristics of each individual scattering center were determined using the concept of a Transient Polarization Response (TPR). Simulations were shown which demonstrate the utility of this technique. One of the technique's greatest advantages over conventional Fourier-based techniques is superresolution. Another advantage is data reduction. Two-Dimensional data sets are inherently large, and this technique obtains pole and amplitude coefficient estimates which contain all of the important target information which form a reduced data set.

6. ACKNOWLEDGMENTS

This research was supported in part by the Air Force Office of Scientific Research and in part by the Avionics Division, Wright Laboratories.

7. REFERENCES

1. J. J. Sacchini, W. L. Steedly, and R. L. Moses, "Two-dimensional prony modeling and parameter estimation," *IEEE Trans. on Signal Processing*, Oct. 1993. (to appear).

2. M. A. Rahman and K. B. Yu, "Total least squares approach for frequency estimation using linear prediction," *IEEE Trans. on Acoustics, Speech, and Signal Processing*, vol. ASSP-35, pp. 1440–1454, Oct. 1987.

3. W. M. Steedly and R. L. Moses, "High resolution exponential modeling of fully polarized radar returns," *IEEE Trans. on Aerospace and Electronic Systems*, vol. AES-27, pp. 459–469, May 1991.

4. N. F. Chamberlain, "Recognition and analysis of aircraft targets by radar, using structural pattern representations derived from polarimetric signatures," June 1989. Also: ElectroScience Laboratory Report 719710-3.

5. J. J. Sacchini, *Development of Two-Dimensional Parametric Radar Signal Modeling and Estimation Techniques with Application to Target Identification.* PhD thesis, The Ohio State University, Columbus, OH, 1992.

6. R. J. Marhefka, "Radar cross section - basic scattering code rcs-bsc (version 2.0) user's manual," Tech. Rep. 718295-15, The Ohio State University, ElectroScience Laboratory, Feb. 1990.

7. J. R. Huynen, *Phenomenological Theory of Radar Targets.* PhD thesis, Technical University Delft, Druckerij Bronder-Offset N.V. Roterdam, Netherlands, 1970.

8. W. M. Steedly and R. L. Moses, "The Cramér-Rao bound for pole and amplitude estimates of damped exponential signals in noise," in *Proceedings of the International Conference on Acoustics, Speech, and Signal Processing*, (Toronto, Ontario), pp. 3569–3572, May 14–17, 1991.

9. P. Stoica, T. Söderström, and F. Ti, "Asymptotic properties of the high-order Yule-Walker estimates of sinusoidal frequencies," *IEEE Trans. on Acoustics, Speech, and Signal Processing*, vol. ASSP–37, pp. 1721–1734, Nov. 1989.

10. R. Kumaresan and D. W. Tufts, "Estimating the parameters of exponentially damped sinusoids and pole-zero modeling in noise," *IEEE Trans. on Acoustics, Speech, and Signal Processing*, vol. ASSP-30, pp. 833–840, Dec. 1982.

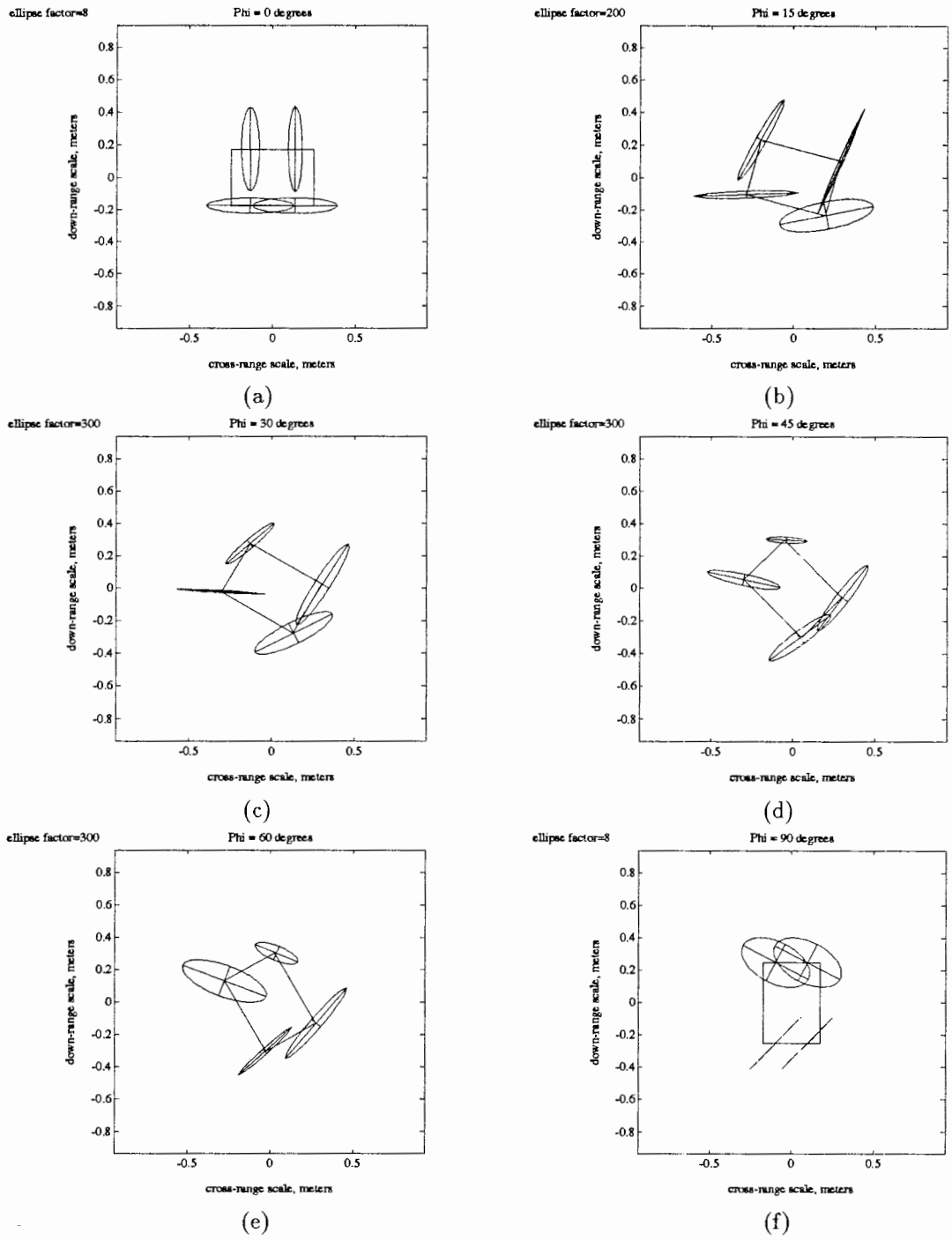

Figure 3: Full polarization flat plate example. Pole locations estimated by FPA2 are located at the centers of the ellipses. The data is a 3° polar swath centered around (a) 0°, (b) 15°, (c) 30°, (d) 45°, (e) 60°, and (f) 90°.